Lattice dynamics and Raman scattering by phonons of GaAs/AlAs(001) superlattices

2009 J. Phys.: Condens. Matter 21 275405

(http://iopscience.iop.org/0953-8984/21/27/275405)

IOP PUBLISHING JOURNAL OF PHYSICS: CONDENSED MATTER

J. Phys.: Condens. Matter **21** (2009) 275405 (14pp) doi:10.1088/0953-8984/21/27/275405

Lattice dynamics and Raman scattering by phonons of GaAs/AlAs(001) superlattices

D Berdekas[1] **and S Ves**[2]

[1] Direction of High Schools Education of Larissa, Lykeio of Giannouli, GR-41500 Larissa, Greece
[2] Physics Department, Aristotle University of Thessaloniki, GR-54124 Thessaloniki, Greece

E-mail: ves@auth.gr

Received 7 November 2008, in final form 1 May 2009
Published 10 June 2009
Online at stacks.iop.org/JPhysCM/21/275405

Abstract

The lattice dynamics of $(GaAs)_n/(AlAs)_n(001)$ superlattices (SLs), $n = 1, 2$, with perfect and disordered (non-perfect) interfaces is studied in detail. The SLs with disordered interfaces are approached by primitive cells, much larger in volume than that of the perfect SL primitive cell. The dynamical matrices of the SLs have been constructed from a combination of the dynamical matrices corresponding to the bulk crystalline constituents, while the interionic forces are calculated by using a ten-parameter valence overlap shell model (VOSM). Furthermore, we calculate the Raman spectra, for both perfect and disordered superlattices by using an eight-parameter bond polarizability model (BPM). Our theoretical results are in very good agreement with the available experimental spectra. Finally, our results clearly demonstrate that intermixing of Ga and Al cations, even to a very small extent, can induce Raman activity, which although not expected in the spectra of perfect superlattices, is actually observed experimentally.

(Some figures in this article are in colour only in the electronic version)

1. Introduction

GaAs/AlAs superlattices (SLs) grown along (001) [1–12], (110) [13], (112), (012) [14] and (111) [15] directions, have been studied in the past by Raman spectroscopy for various layer configurations. The experimental studies on (001) SLs are mainly focused on the investigation of the intensities of the longitudinal modes. From the point of view of lattice dynamics, (001) grown SLs have also attracted considerable attention, approached mainly by qualitative models, such as the linear chain model [1, 12] or the elastic [16] and dielectric [17] continuum models. Calculations, based on three-dimensional models, and trying to give a more realistic insight into these compounds [18–26], also exist. In particular, in the case of short period $(GaAs)_n/(AlAs)_n(001)$ SLs, some of these calculations have considered disordered interface layers [3, 19, 21, 22, 25, 26] without avoiding, for some of them, several questionable approximations or unrealistic results. For example, in [3] two separate parameter sets are used, one for GaAs and one for AlAs. The latter set has been obtained by fitting the eleven-parameter rigid ion model (RIM) to a very small number of experimental data. Furthermore, in the same work [3] a larger cation intermixing depth in 1×1 SL was found than in 5×5 SL, in contrast to what could be expected. In [19] only the frequencies of the GaAs layer are discussed, while remarkable deviations from experiment have been obtained for the highest frequency LO modes for the monolayer and bilayer SLs. In the same work, a few Raman lines obtained by the coherent potential approximation (CPA) are restricted to the bulk GaAs optical frequency range, while the obtained spectral lines are in poor agreement with the corresponding experimental lineshapes. Also, in [21] is studied the influence of a special type of interface disorder on the frequencies and the localization of GaAs optical modes without estimation of Raman spectra. Also the, rather contrived, type of interface disorder considered in [25, 26] has given frequencies far away from the experimental ones, especially for 1×1 SLs.

Finally, in [3] and [12] are presented calculations of Raman spectra of short-period SLs, based also on versions of the bond polarizability model far away from resonance conditions. Their theoretical Raman spectra, although in arbitrary units, reproduce rather roughly, especially in [3], the basic features of the experimental spectra for some $(GaAs)_n/(AlAs)_n(001)$ SLs [3, 12, 26]. In both aforementioned works ([3, 12]), the estimated Raman

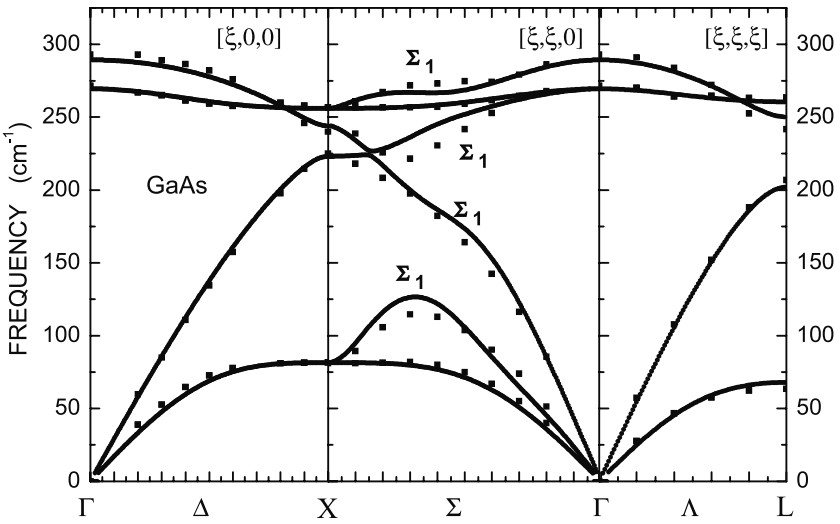

Figure 1. Phonon dispersion curves of GaAs calculated by the ten-parameter VOSM model (solid lines). The solid points denote experimental data [33].

intensities are obtained based on the ambiguous hypothesis that the polarizability parameters of the Al–As bonds are about three times smaller than those of Ga–As. However, this hypothesis is not supported by other works [27]. In [26] an oversimplified approximation is used for the calculation of the Raman intensities for a 5 × 5 SL without any comparison with experiment.

In the present study initially we used the ten-parameter VOSM [28, 29], with slightly improved valence force field [30], to obtain the vibrational modes of the bulk crystals GaAs and AlAs. In particular, for the SLs with perfect interfaces, we use the proper primitive cell, which is for the 1 × 1 (2 × 2) SL two (four) times larger the volume of the primitive cell of the zinc blende structure. For SLs with disordered interfaces, we use much larger primitive cells. The primitive cell of the perfect 1 × 1 SL contains one layer of GaAs and one layer of AlAs, while for the non-perfect 1 × 1 SL we use primitive cells containing 20 and 40 layers of both GaAs and AlAs constituents which do not follow the expected layer sequence. Also, we use cells with 64 and 128 atoms with Ga (Al) layers containing Al (Ga) to a small extent. This is what we call cation intermixing. We follow an analogous situation for 2 × 2 SL. Afterward, the SL short and long range interactions are estimated from the interactions of the constituent bulk crystals by exploiting a similarity transformation method [18]. In all the above cases, we have calculated the corresponding Raman spectra, using the bond polarizability model [31, 32] with values for the bond polarizability parameters able not only to reproduce as good as possible the relative Raman intensities, but also to give realistic values for them.

2. Calculation of the GaAs and AlAs interionic forces

As mentioned above, for obtaining the vibrational modes of the bulk GaAs crystal we used a ten-parameter VOSM model, modified for a better description of the valence bond bending forces [30]. The VOSM model involves three electric parameters Z, Y_1 and Y_2, which account for the long range interactions, two core–shell coupling parameters k_1 and k_2, and five valence force field parameters, one bond stretching parameter λ and four bond bending parameters $k_{r1\theta}$, $k'_{r1\theta}$, $k_{r2\theta}$ and $k'_{r2\theta}$ for expressing the short range interactions. The values of these parameters are estimated by a least-squares fitting to the existing experimental phonon data for GaAs [33]. The best fit values found are: $Z = 2$ (kept constant), $Y_1 = 6.285$, $Y_2 = -2.455$, (in proton charges), $k_1 = 16.84$, $k_2 = 5.516$, $\lambda = 2.387$, $k_{r1\theta} = 0.44$, $k'_{r1\theta} = -0.358$, $k_{r2\theta} = -0.201$ and $k'_{r2\theta} = 0.14$ (in 10^2 N m^{-1}). This parameter set is very similar to that found earlier [22] by fitting to the experimental frequencies of Dolling [34]. The phonon dispersion curves calculated with the above parameter set along the main directions is shown by solid lines in figure 1, while the solid symbols indicate the experimental frequencies. Except for some small discrepancies along the Σ direction, with the pronounced ones along the branches labeled by Σ_1, the overall fitting is very satisfactory. The mean standard deviation is 4.25 cm^{-1}. Parameter sets for GaAs obtained with an older version of the VOSM [28] are also reported in [33]. Despite the fact that they give phonon dispersion curves with mean standard deviations close to that obtained by our set of parameters, it was impossible for us to obtain with these sets reasonable phonon dispersion for other III–V compounds, for instance GaP and GaSb.

Unfortunately, for AlAs there exist experimental data only at the Γ and X [35] points of the Brillouin zone. Because of the very few existing experimental frequencies for AlAs, several authors have tried to obtain additional frequencies for the bulk AlAs crystal from the AlAs-like modes present in the Raman spectra of GaAs/AlAs(001) [1, 3–5, 26]. The argument used is that all the modes present in the Raman spectra originate barely from the [00ξ] direction, and that all the AlAs-like modes have been activated by folding. In this way, the phonon dispersion of LO and TO modes along the Δ direction is reproduced. This dispersion has been used to obtain, by least squares, a

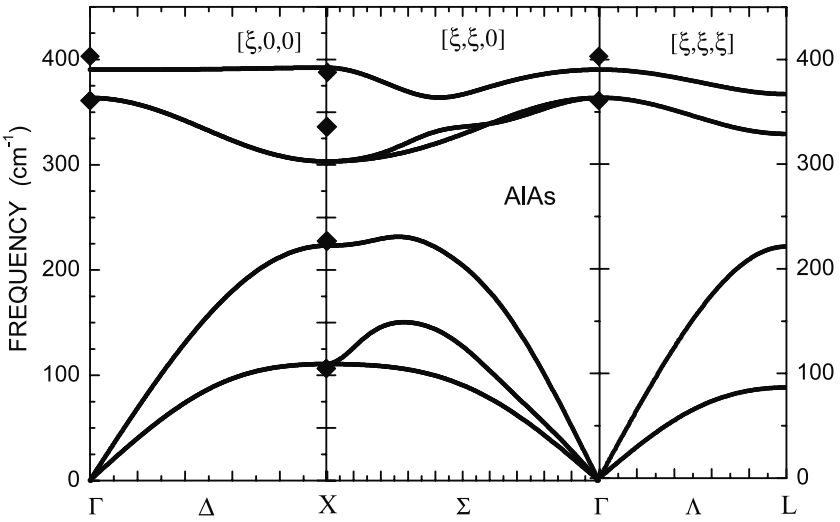

Figure 2. Phonon dispersion curves of AlAs calculated by the ten-parameter VOSM model (solid lines). The solid points denote experimental data [35].

set of parameters for AlAs. But if even these assumptions were true, the dispersion along the Δ direction alone is not sufficient for obtaining a reliable parameter set for any crystal compound. So, in order to estimate the phonons of AlAs, we believe that scaling the dynamical matrix elements of GaAs by just substituting the Ga mass by the Al mass is more reliable and consistent. Under this assumption, the obtained dispersion curves for AlAs, along with available experimental data, are displayed in figure 2 for the main directions.

3. Calculation of phonon dispersion for $(GaAs)_1/(AlAs)_1(001)$ SL

The dynamical matrix for the SL are constructed by combining properly the 6×6 dynamical matrices of the bulk constituents GaAs and AlAs calculated at certain points of the Brillouin zone [18]. In particular, we define a new unit cell, a supercell, which is N times larger than the corresponding zinc blende primitive cell. This supercell is the SLs primitive cell. The dynamical matrix for each bulk constituent is calculated using the supercell. The dimension of the new dynamical matrix for the bulk crystal is $6N \times 6N$ and can be expressed in terms of the 6×6 dynamical matrix of the bulk crystal, referred to the primitive zinc blende cell. The 6×6 dynamical matrices are calculated at certain points of the original Brillouin zone, which are folded back to the center of the new Brillouin zone. Finally the $6N \times 6N$ dynamical matrix is properly transformed [18] to give the SLs dynamical matrix.

In figure 3 are displayed the calculated phonon dispersion curves for the 1×1 SL GaAs/AlAs(001) along the directions $(\xi\xi 0)$ (left) and (00ξ) (right). Directions $(\xi, 0, 0)$, $(0, \xi, 0)$ and $(0, 0, \xi)$ coincide with Cartesian x, y, z axes defined by the corresponding zinc blende unit cell. In the middle panel is displayed the phonon angular dispersion at the Γ point, as it is approached with zero wavevector and varying from (00ξ) to $(\xi\xi 0)$. This is Γ–θ–Γ dispersion with the angle θ varying from 0 to $\pi/2$. When the Γ point is approached from a direction parallel to the growth direction ($\theta = 0$), the point group of the wavevector $G_o(\mathbf{k})$ is D_{2d} and correspondingly the vibrational modes are distributed within the irreducible representations $A_1 + 3B_2 + 4E$ (A_1 longitudinal symmetric, B_2 longitudinal, E transverse). Along the (00ξ) direction, with ξ different from zero, the group of the wavevector $G_o(\mathbf{k})$ is the C_{2v} of the orthorhombic system, while the irreducible representations of the modes are $4A_1 + 4B_1 + 4B_2$ (A_1 symmetric longitudinal, B_1, B_2 transverse). In the case where Γ is reached from the $(\xi\xi 0)$ direction, the group of the wavevector $G_o(\mathbf{k})$ is the C_S of the monoclinic system. In this case, the modes of vibration are distributed to the irreducible representations $8A' + 4A''$. The A′ modes are mixed modes and the atomic displacements have components along the x and z directions. Going from $\theta = 0$ [(00ξ) direction] to $\theta = \pi/2$ [$(\xi\xi 0)$ direction], due to the lowering of the symmetry, the pure longitudinal modes are mixed modes and consequently the macroscopic produced field decreases, resulting also in a lowering of the A′ mode frequencies. On the other hand, the branches of the A″ modes, which are transverse modes with atomic displacements along the y direction, are almost dispersionless, owing to the fact they do not create a macroscopic field.

Previous calculations of the phonon dispersion curves along the Δ direction [18] for 1×1 SL (001) gave unsatisfactory results, with the main discrepancy the LO–TO frequency inversion, i.e. the TO frequencies of the modes for both GaAs and AlAs layers obtained at higher frequencies than the corresponding LO mode frequencies.

4. The Raman spectra

The Raman scattering intensity is proportional to the fourth rank tensor $I_{\alpha\beta\gamma\delta}$, which is given by the expression [36]

$$I_{\alpha\beta\gamma\delta} = \sum_j R_{\alpha\beta\gamma\delta}(0j)\delta(\omega - \omega_j) \qquad (1)$$

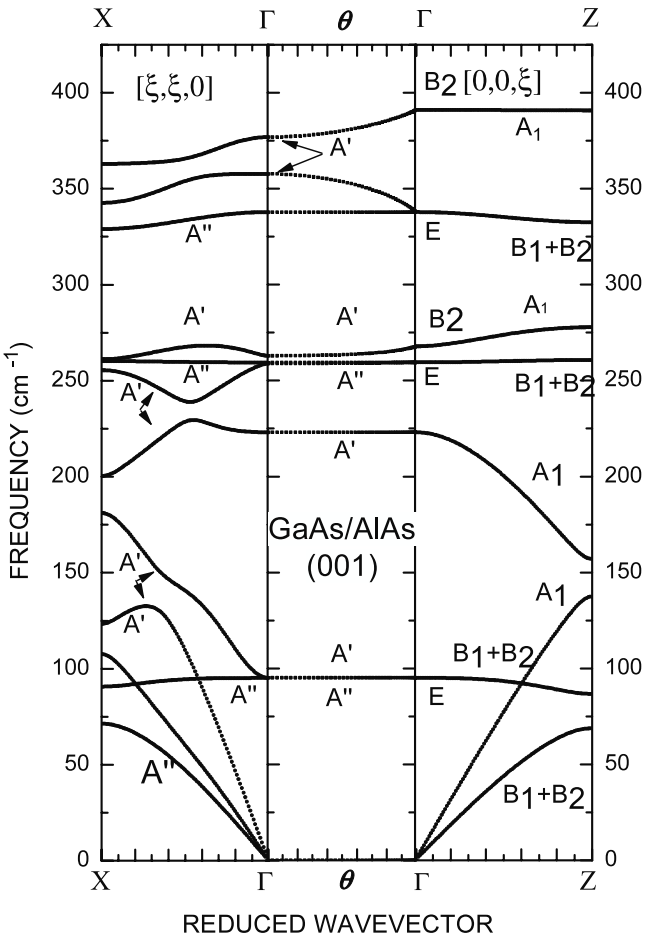

Figure 3. Phonon dispersion curves for 1×1 perfect GaAs/AlAs(001) SL calculated by the ten-parameter VOSM model.

where $R_{\alpha\beta\gamma\delta}(0j)$ is the Raman strength of the jth mode at zero wavevector, given by

$$R_{\alpha\beta\gamma\delta}(0j) = \alpha_{\alpha\beta}(0j)\alpha_{\gamma\delta}(0j)[\eta(\omega_j+1)] \tag{2}$$

with $\alpha_{\alpha\beta}(0j)$ being the first-order polarizability derivative of the electronic polarizability of the ω_j mode and $\eta(\omega_j)$ is the Bose–Einstein factor:

$$\eta(\omega_j) = \frac{1}{e^{\frac{\hbar\omega_j}{kT}} - 1}. \tag{3}$$

The function $\delta(\omega - \omega_j)$ is approximated by the Lorentzian [36]

$$\delta(\omega - \omega_j) = \frac{1}{\pi}\frac{\Gamma_j}{[(\omega - \omega_j)^2 + \Gamma_j^2]} \tag{4}$$

where Γ_j is the half-width at half-maximum (HWHM) of the j mode with frequency ω_j.

The first-order polarizability derivative of the electronic polarizability of the mode ω_j with respect to the corresponding normal coordinate is given by

$$\alpha_{\alpha\beta}(0j) = \sqrt{\frac{\hbar}{\omega_j}}\sum_n\sum_\rho\left(\frac{\partial\alpha_n}{\partial\rho_\kappa}\right)_{\alpha\beta}[u_\rho(\kappa|0j) - u_\rho(\kappa'|0j)] \tag{5}$$

where n runs over all the bonds in the unit cell, $\rho = x, y, z$ and $u_\rho(\kappa|0j)$ is the displacement of the atom κ in mode j with zero wavevector.

The changes of the polarizability for each bond are calculated using the bond polarizability model. According to this model for each bond, besides the atomic displacements, are also required the parallel, α_p, and vertical, α_v, components of the polarizabilities relative to the bond axis, as well as their derivatives α'_p, α'_v with respect tp the bond length change. The number of unknown parameters can be reduced if we take into account the following two relations [37]:

$$\alpha_p + 2\alpha_v = \frac{3V}{16\pi}(\varepsilon_\infty - 1) \tag{6}$$

$$\alpha_p/\alpha_v = 1.1 \tag{7}$$

where V is the primitive cell volume of the bulk crystal and ε_∞ is the high frequency dielectric constant. Relation (7) holds, approximately, only for III–V binaries [37].

The values of the four parameters α_p, α_v, α'_p and α'_v for Ga–As and Al–As bonds are estimated, taking into account not only equations (6) and (7), but also the constraint that the Raman polarizability for the TO mode of GaAs has to range from about 50×10^{-16} cm^2 [38] to 100×10^{-16} cm^2 [39]. By least-squares fitting of the theoretical expressions to the experimental Raman intensities for the 1×1, 2×2, 3×3, 4×4 GaAs/AlAs(001) SLs, we obtained the bond parameters: (a) for the Ga–As bonds: $\alpha_p = 8.7$ (10^{-24} cm^3), $\alpha_v = 9.0$ (10^{-24} cm^3), $\alpha'_p = 1.5$ (10^{-16} cm^2), $\alpha'_v = 0.6$ (10^{-16} cm^2). (b) For the Al–As bonds $\alpha_p = 6.9$ (10^{-24} cm^3), $\alpha_v = 6.7$ (10^{-24} cm^3), $\alpha'_p = 0.8$ (10^{-16} cm^2), $\alpha'_v = 0.5$ (10^{-16} cm^2). Throughout our calculations we have used for HWHM 4 cm^{-1} and 10 cm^{-1} for modes with frequencies above and below 230 cm^{-1}, respectively, and the X, Y, Z unit cell—supercell axes coinciding with those defined by the zinc blende unit cell. For SLs thicker than 1×1 SL, for comparison reasons, we have divided the Raman intensities by the number of times the 1×1 unit cell is contained in the SL's unit cell. In the following, as concerns the Raman strength R, we used the two-indices notation, e.g. $\alpha\beta = \gamma\delta$

5. Results and discussion

5.1. (GaAs)1/(AlAs)1(001) perfect SL

Figure 4 (solid lines) displays the calculated Raman spectrum for the 1×1 GaAs/AlAs(001) superlattice (figure 5(a)) with ideal interfaces. The calculation is made for the modes active in the backscattering geometry $Z(X + Y, X + Y)\bar{Z}$ and for wavevector along the superlattice axis approaching zero. In the $Z(X + Y, X + Y)\bar{Z}$ geometry can be detected both A_1 and B_2 longitudinal modes. The two strong peaks d and e correspond to the LO(Γ) of GaAs at 267.8 cm^{-1} and LO(Γ) of AlAs at 391 cm^{-1}. The corresponding experimental peaks (dotted lines) appear at 275 cm^{-1} and 385 cm^{-1} for GaAs and AlAs, respectively [9]. The peak b′ at 223 cm^{-1} corresponds to the longitudinal A_1 mode, where only the As atoms are moving one against each other. This mode originates from the folding

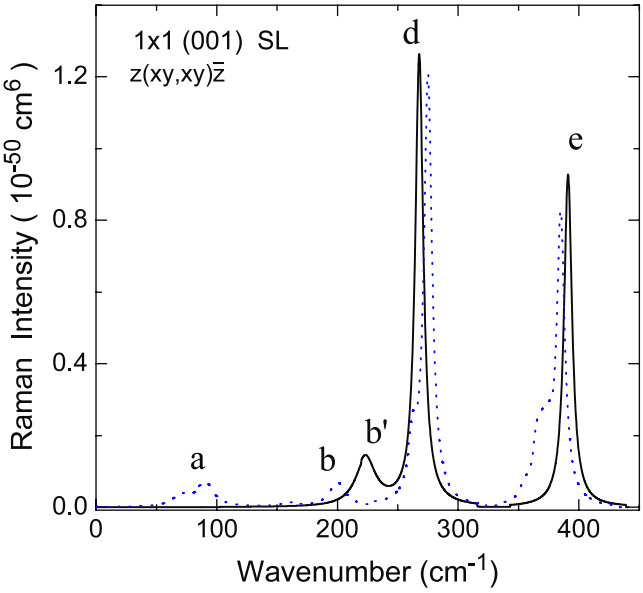

Figure 4. Raman spectrum for the perfect GaAs/AlAs(001) calculated by the bond polarizability models using a 12 × 12 supercell.

of the LA(X) mode and it is expected to be active only for all (001) Sls, with odd numbers of layers from each constituent. The experimental frequency of this mode is very close to 227 cm^{-1} for both GaAs [33, 34] and AlAs bulk crystals [35].

At the left of the calculated peak b′ appears the peak b of the experimental spectrum close to 200 cm^{-1}. The peak b has been attributed [1, 7, 9, 10, 12], up to now, to the folded activated LA(X) mode. Even the frequency of that mode was recognized to be very close to the LA(L) mode [12]. Simple linear chain model calculations [12] have estimated the frequency of this mode at 198 cm^{-1} and arbitrary values for the polarizability tensors α_{xy} were used. So, the Raman strength of this A_1 mode has been found to be several times larger than the strength of LO(Γ) of GaAs [12]. Although these polarizability values are unrealistic, they have also been used to obtain the Raman spectra for GaAs/AlAs SLs grown along the (113) direction [40].

With the exception of the good agreement between calculated and experimental spectrum intensities of the two strong optical B_2 modes of LO (Γ) of GaAs and LO (Γ) of AlAs, a closer examination reveals several discrepancies compared to the experimental spectrum. For example, in the calculated spectrum are not reproduced the left asymmetries of the lineshapes of both the confined LO(Γ) modes. For example, apart from the A_1 mode at 223 cm^{-1} (peak b′), no other peaks are present in the acoustic frequency range, neither close to the peak at 200 cm^{-1} nor close to 80 cm^{-1}, where there appears clearly a peak in the experimental spectrum. The disagreement between predicted active modes and those observed in the experimental Raman spectra were very often attributed to deviations from strict backscattering geometry [1]. But even for large deviations from strict backscattering geometry, up to 30°, the laser beam travels very close to the SL axis due to the large refractive index of the Sl,

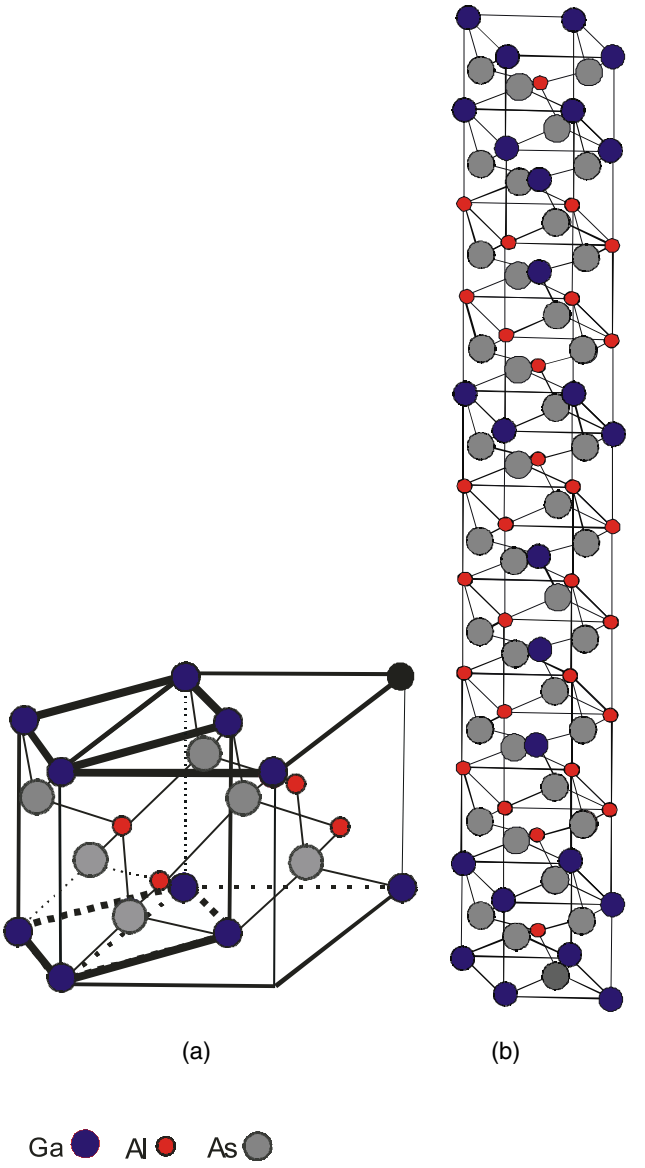

Figure 5. (a) Unit cell and primitive cell (denoted by bold lines) for GaAs/AlAs(001) 1 × 1 perfect SL. (b) Supercell describing a disordered layer sequence GaAs/AlAs(001) 1 × 1 SL containing 20 layers (10 from GaAs and 10 from AlAs).

which is about 3. This fact is also demonstrated in figure 3, middle panel, where the frequencies of most of the modes remain practically unaltered for angles smaller than 45°.

5.2. (GaAs)1/(AlAs)1(001) disordered layer superlattices (DLSLs)

To resolve the discrepancies and get a better insight of the experimental spectrum, we consider a new larger elementary cell, ten times bigger than the elementary cell of the perfect Sl. It contains 10 GaAs layers and 10 AlAs layers along the SL axis and it is displayed in figure 5(b). In this bigger cell, the layers of GaAs and AlAs do not follow the sequence of layers of the perfect 1 × 1 SL, but we have interchanged the positions for about half of them. In particular, the new disordered sequence

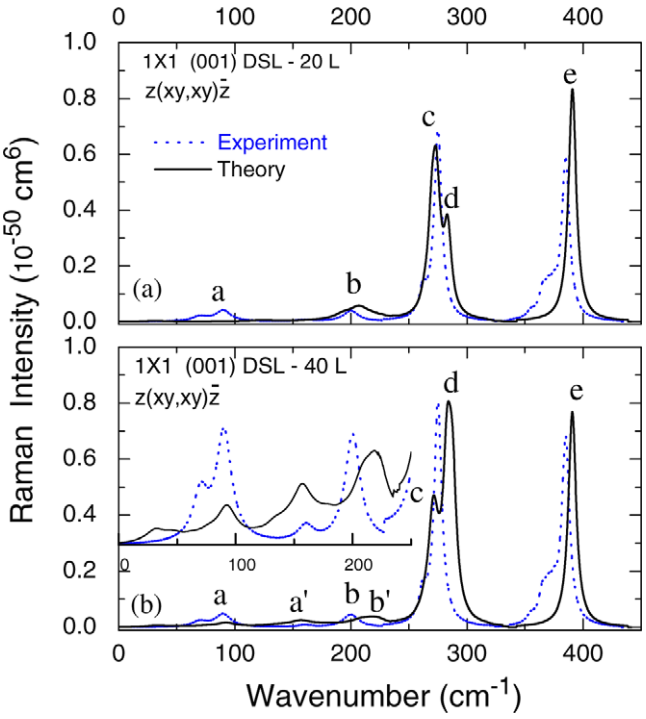

Figure 6. Calculated Raman spectra for disordered layer sequence GaAs/AlAs(001) (a) with 20 layers and (b) with 40 layers. The x, y, z axes designate the zinc blende unit cell axes.

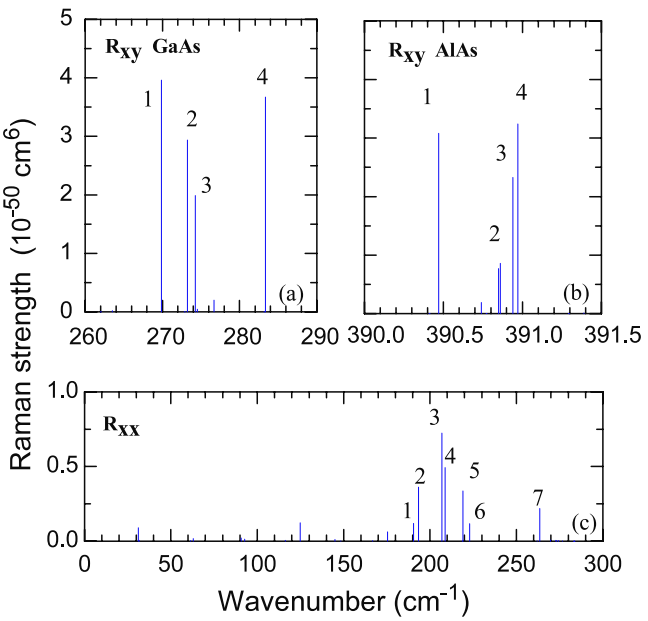

Figure 7. Calculated Raman mode strengths for the disordered layer sequence 1 × 1 GaAs/AlAs(001) SL with 20 layers. (a) Longitudinal GaAs modes, (b) longitudinal AlAs modes, (c) longitudinal modes below 300 cm^{-1}.

is GaAsAlAs/GaAsGaAs/AlAsGaAs/AlAsGaAs/AlAsGaAs/AlAsAlAs/GaAsAlAs/AlAsGaAs/AlAsGaAs/GaAsAlAs/.

In this case, the points of the original Brillouin zone, which are folded back to the center of the new one, are points along the $(0, 0, \xi)$ direction that fulfill the relation

$$\xi = \frac{2}{n+m}\zeta \tag{8}$$

with $\zeta = 0, 1, 2, 3, \ldots (n + m - 1)$[3]. The 6 × 6 dynamical matrices for bulk GaAs are calculated at all these points and, after similarity transformation matrix and mass replacement for Al atoms, we obtain a 120 × 120 SL dynamical matrix, which means 120 vibrational modes for this SL. The individual modes are distributed as follows: 30 of these modes are located in GaAs layers and 30 of them are located in AlAs layers. Ten of these 30 modes are longitudinal and 10 of them are transverse modes, doubly degenerate. The remaining 60 modes are acoustic modes extended to both kinds of layers, 20 of them longitudinal and 20 transverse doubly degenerate modes. The same analysis holds also for the case when more layers are included in the elementary cell. For example, in the case of 20 layers of each constituent, the dynamical matrix has dimensions 240 × 240, which means 240 vibrational modes for this SL. Consequently, besides the considerably demanding computational effort, the number of modes in each species is also doubled.

The calculated (solid line) and experimental (dotted line) Raman spectra for the longitudinal modes of disordered layered superlattices (DLSL) comprised by 20 and 40 layers are shown in figures 6(a) and 6(b), respectively. In particular, the spectrum in figure 6(b) has been obtained by using a primitive cell containing 20 GaAs layers and 20 AlAs layers along the SL axis at the following disordered layers sequence: GaAsAlAs/AlAsAlAs/GaAsGaAs/AlAsGaAs/AlAsGaAs/AlAsGaAs/GaAsAlAs/AlAsGaAs/GaAsGaAs/GaAsGaAs/AlAsAlAs/GaAsAlAs/GaAsAlAs/GaAsAlAs/AlAsAlAs/GaAsGaAs/GaAsAlAs/GaAsGaAs/AlAsGaAs/GaAsAlAs.

The calculated Raman spectrum of longitudinal modes, active in the backscattering geometry Z(X + Y, X + Y)$\bar{Z}$, for the DLSL containing 10 layers of GaAs and 10 layers of AlAs is shown in figure 6(a). In the optical frequency range of GaAs appear two peaks: one stronger at 274.3 cm^{-1} and a weaker one at 283.4 cm^{-1} (peaks c and d, solid lines, figure 6(a)). Peak c contains the contributions of the modes at 269.9 cm^{-1}, 273.2 cm^{-1}, 274.3 cm^{-1}, with strengths marked by 1, 2, 3 in figure 7(a), respectively. Here, we should notice that the mode at 263.5 cm^{-1}, marked by 7 in figure 7(c), is a longitudinal mode. Even its frequency is very close to the TO(Γ) mode of bulk GaAs. Peak d corresponds to the mode at 283.4 cm^{-1} (labeled as 4 in figure 7(a)), which is also a strong mode in this frequency range. In this mode the Ga and As atoms of two consecutive GaAs layers (3th–4th and 18th–19th layers) move with large displacements along the z axis. The presence of these two GaAs groups results in a mode with its frequency raised closer to the frequency of the LO(Γ) mode of bulk GaAs. Furthermore, figure 7(a) shows clearly, that only four GaAs longitudinal optical modes have significant strengths. Finally, we mention that all the 10 GaAs located longitudinal optic modes are predicted to be Raman-active.

In the optical frequency range of AlAs peak e at 390.97 cm^{-1} (solid line, figure 6(a)) is formed mainly from contributions of the modes at 390.5 cm^{-1}, 390.85 cm^{-1},

[3] In our case $n + m - 1 = 20 - 1 = 19$. (Times $2\pi/a$, a = lattice constant of the zinc blende unit cell.)

390.94 cm^{-1} and 390.97 cm^{-1}, labeled, respectively, as 1, 2, 3 and 4 in figure 7(b). We point out that, as in the case of GaAs, only four out of ten AlAs longitudinal optical modes have significant strengths.

Finally, it should be mentioned that in the calculated spectrum of figure 6(a) no peak is found close to 80 cm^{-1}. Even the peak at 223 cm^{-1}, due to the activated mode LA(X), is absent. By comparing figures 4 and 6(a), it is clearly revealed the strong dependence of the strength of this mode on the layer sequence; in figure 4 this mode appears at full strength while in figure 6(a) it is attenuated by the disorder. Indeed, instead of the peak b′, at 223 cm^{-1} (figure 4), appears peak b at 206.9 cm^{-1} (figure 6(a)). This new peak is formed by the contributions of four longitudinal modes at 190.5, 193.4, 206.9 and 208.7 cm^{-1}. Their strength distribution is shown in figure 7(c) (labeled as 1, 2, 3 and 4, respectively). Notice the strength domination of the modes at 193.4 and 206.9, which are almost two to three times stronger compared to the strength of the activated mode LA(X) at 223 cm^{-1} (labeled as 6 figure 7(c)). The frequencies of the acoustic longitudinal modes of bulk GaAs (AlAs) from the $(0, 0, \xi)$ direction are: for $\xi = 0.7$, 181.8 cm^{-1} (198.4 cm^{-1}), for $\xi = 0.8$, 200.3 cm^{-1} (212.0 cm^{-1}), respectively. The mean values of the above frequencies are 190.1 cm^{-1} and (206.2 cm^{-1}), respectively. Therefore, we anticipate that the modes with frequencies 190.5 cm^{-1} and 193.4 cm^{-1} originate from the (0, 0, 0.7) point and the modes 206.9 cm^{-1} and 208.7 cm^{-1} from the (0, 0, 0.8) point of the Brillouin zone, respectively.

Coming back to panel b of figure 6, displaying the calculated intensities of longitudinal modes active in the backscattering geometry $Z(X + Y, X + Y)\bar{Z}$, we see that the optical range of GaAs is dominated by the strongest peak at 283.7 cm^{-1} (peak d, solid line). At the left of this mode appears a weaker longitudinal mode at 271.5 cm^{-1} (peak c, solid line) which modifies the symmetric profile of the GaAs-like LO(Γ) mode to an asymmetric one. To both peaks c and d contribute about six strong modes dispersed from 269.8 to 287.9 cm^{-1} and labeled from 1 to 8 in figure 8(a). In total, in the optical frequency of bulk GaAs there exist 20 GaAs-like longitudinal modes, but less than half of them have significant strengths (figure 8(a)), which means that the weak modes would be hardly traced in the experimental spectrum. Furthermore, some of them are very close each other, like those at 269.8 and 271.5 or those at 282.5 and 283.1 in figure 8(a), rendering the situation more complicated and uncertain. Therefore, an unambiguous assignment of the above modes to certain points of the $(0, 0, \xi)$ dispersion of bulk GaAs is not possible. Similarly, the strong peak e at 390.97 cm^{-1}, solid line in figure 6(b), lying in the optical frequency range of AlAs, is formed by several modes. They are spread from 390.3 to 391.6 cm^{-1}, labeled by 1–5, figure 8(b), and with the strongest one at 390.33 cm^{-1}. We mention that the clustering of all the AlAs LO-like modes at frequencies about 391 cm^{-1} is due to the almost dispersionless LO branch of bulk AlAs (figure 2). From the above findings, we conclude that it should be very difficult to trace all the active modes in the Raman spectrum, since each peak is formed by several modes, very close one to another. This is in contrast to previous works [4, 5, 26] which

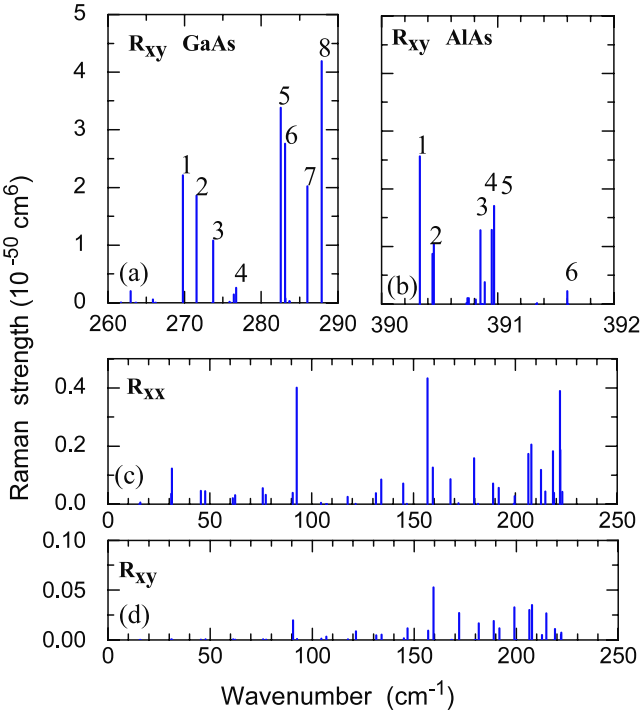

Figure 8. Calculated Raman mode strengths for the disordered layer sequence 1 × 1 GaAs/AlAs(001) SL with 40 layers. (a) Longitudinal GaAs modes, (b) longitudinal AlAs modes, (c) longitudinal modes below 250 cm^{-1}, (d) longitudinal modes below 250 cm^{-1}.

tried to assign consecutive weak SL Raman-active modes to bulk modes of certain consecutive wavevectors.

Finally, also the spectrum in the acoustic range is now much closer to the experimental one. Peak a, solid lines, figure 6(b), appears at 92.2 cm^{-1}, while a new weak peak a′ at 156.5 cm^{-1} comes into sight, with contributions from the weaker modes close to 155 cm^{-1}. The longitudinal modes at 92.2 cm^{-1} and 156.5 cm^{-1} originate from the $\xi = 0.3$ and $\xi = 0.55$ points along the $(0, 0, \xi)$ direction, respectively. The peak b′ in the calculated spectrum appears at 222 cm^{-1} (solid line, figure 6(b)) and it contains contributions from the weak modes at 206.4, 207.8, 221.8 and 222 cm^{-1} (see also figure 8(c)). The former two originate from the $\xi = 0.8$ point, while the latter two from the $\xi = 0.95$ point of the Brillouin zone. It should be noticed that the majority of the longitudinal modes originating from the $\xi = 0.8, 0.85, 0.9, 0.95$ points are active, figure 8(c). The strength of the activated LA(X) mode is small compared to the strengths of the modes at 222 cm^{-1} because the strength of the mode at 223 cm^{-1} does strongly depend on the sequence of the constituent layers of the SL.

5.3. $(GaAs)_1/(AlAs)_1(001)$ SLs with disordered lattice sites (cation intermixing)

5.3.1. Supercell with 64 atoms. As a next step, we described the 1 × 1 SL with an even larger elementary cell defined by

$$\mathbf{a}_1 = 2a\mathbf{i} \qquad \mathbf{a}_2 = 2a\mathbf{j} \qquad \mathbf{a}_3 = 2a\mathbf{k}$$

where $a = 5.65$ A. This new cell contains 8 zinc blende unit cells (figure 9(a)), two along each axis Each lattice plane

Table 1. Calculated frequencies in the overlapping acoustic region of the bulk GaAs and AlAs, along with the degeneracy at specific points of the Brillouin zone.

Point	Degeneracy	GaAs frequency (cm^{-1})	AlAs frequency (cm^{-1})	Mean frequency (cm^{-1})
(0.50, 0.50, 0.50)	8	67.9	86.5	77.2
(0.00, 0.00, 0.50)	12	68.8	86.7	77.7
(0.50, 0.50, 0.00)	12	71.3	90.6	81.0
(0.00, 0.00, 1.00)	6	81.5	110.6	96.0
(1.50, 0.50, 0.00)	6	87.5	112.9	100.2
(0.50, 0.50, 0.00)	12	105.9	127.5	116.7
(0.00, 0.00, 0.50)	6	137.4	157.0	147.2
(1.00, 0.50, 0.00)	6	141.8	170.6	156.2
(0.50, 0.50, 0.00)	12	173.5	204.4	189.0
(0.50, 0.50, 0.50)	4	201.8	221.0	211.4

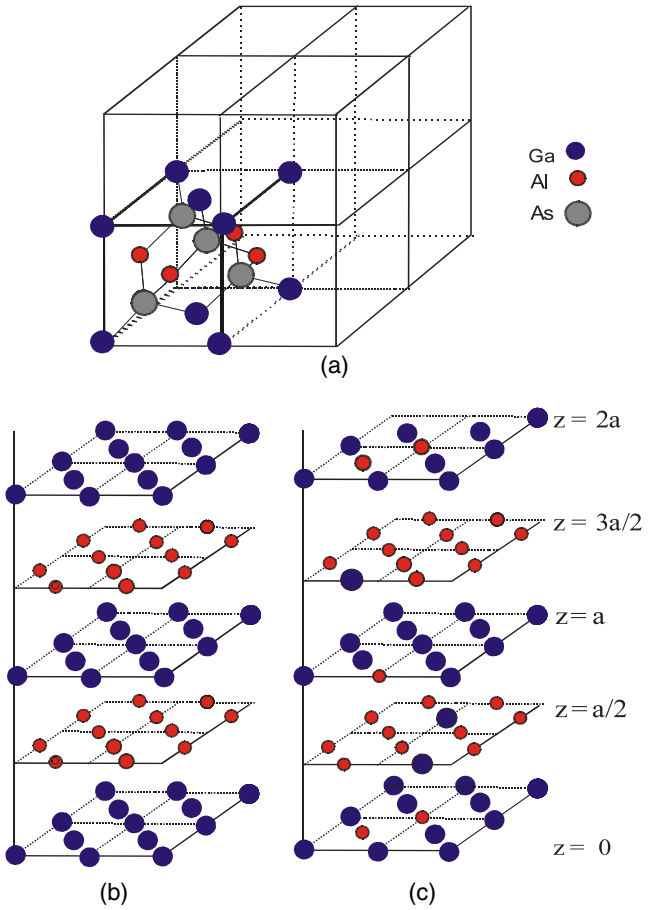

Figure 9. (a) Supercell containing 8 zinc blende unit cells (2 along each axis). Translation of the tetragonal unit cell (lower left corner) in space reproduces the structure of the perfect GaAs/AlAs(001) SL. (b) Alternating Ga and Al cation lattice planes of the supercell defined in (a) while in (c) these cation planes contain both Ga and Al (cation intermixing).

contains 8 cations and 8 anions, and the new cell contains in total 32 cations and 32 anions. Furthermore, instead of the pure layers considered before, we now introduce a small degree of cation intermixing, which means that each lattice plane along the z direction is an Al_xGa_{1-x} alloy plane (figure 9(b)) as follows. At the start, we assume that the first layer (0, 0, 0) contains 6 atoms of Ga and 2 atoms of Al ($x = 0.25$). The second cation layer is the lattice plane at $(0, 0, a/2)$ that contains 2 atoms of Ga and 6 atoms of Al ($x = 0.75$). The next cation layer at height $z = a$ contains 7 Ga cations and 1 Al cation ($x = 0.125$). Finally the layer at height $z = 3a/2$ contains 7 Al cations and 1 Ga cation. The symmetry space group of the 64-atom cubic unit cell is the C_1 space group of the triclinic system because this cell does not contain any symmetry operation element. Consequently none of the modes is either purely longitudinal or purely transverse modes but all are mixed modes which belong to the A irreducible representation. In this case, the points of the original Brillouin zone which are folded to the center of the new smaller Brillouin zone are: (a) the Γ point (0, 0, 0), (b) six points from the Δ direction equivalent to the point (0.5, 0, 0), (c) three points equivalent to the X point, (d) four points equivalent to the L point, (e) twelve points from the Σ direction (0.5, 0.5, 0) and (f) six points from the Z direction equivalent to the W point. Finally there is constructed a 192 × 192 SL dynamical matrix which is solved to obtain the eigenvectors and eigenfrequencies of the disordered SL. Within this description there exist 96 modes in the acoustic frequency range of the bulk constituents, 48 modes in the optical frequency range of GaAs and 48 modes in the optical frequency range of AlAs. In order to identify the origin of the SL modes in the bulk acoustic range, we construct table 1. In table 1 are given the calculated frequencies in the overlapping acoustic region of the bulk GaAs (third column) and AlAs (fourth column) in ascending order. In the first two columns are given the point of the Brillouin zone and its degree of degeneracy. In the fifth column is given the mean frequency for each point. So, for the SL modes in the acoustic range of the bulk constituents we expect, in ascending order, eight modes originating from the (0.5, 0.5, 0.5) point, twelve modes originating from the (0, 0, 0.50) point and so on.

The same procedure cannot be safely applied for the modes in the optical frequency range of the bulk constituents because, apart from the close proximity of the mode frequencies, the cation intermixing affects the *mainly longitudinal* modes in a different way with respect to the *mainly transverse* modes. The mainly longitudinal ones are shifted towards smaller frequencies since the macroscopic field of the GaAs (AlAs) modes is decreased by the presence of Al (Ga) atoms in the same lattice plane. The mainly transverse GaAs (AlAs)-like ones tend to slightly higher

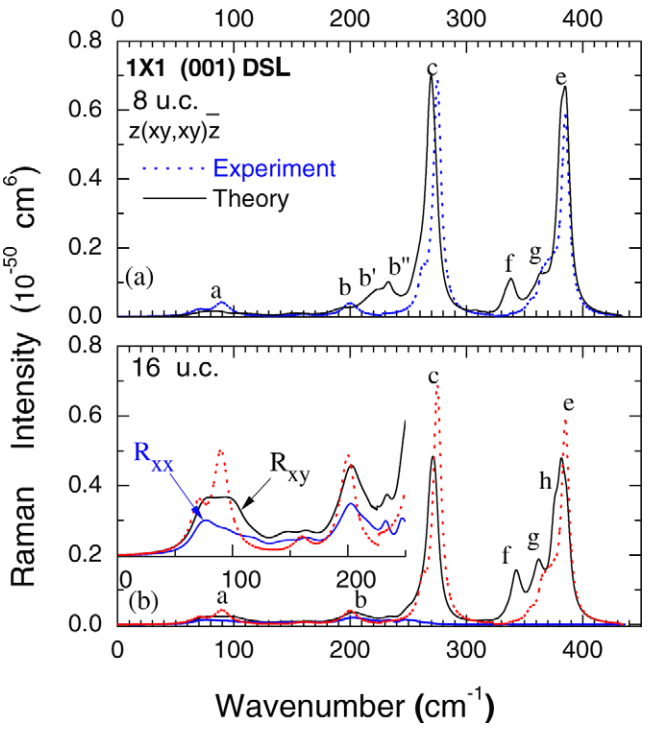

Figure 10. Raman spectra (solid lines) for GaAs/AlAs(001) with cation intermixing calculated with primitive cell containing (a) 8 zinc blende unit cells and (b) 16 zinc blende unit cells. Dotted (a) and dashed (b) lines refer to the corresponding experimental spectrum. In the inset in (b) are redrawn the R_{xx} and R_{xy} activities for clarity.

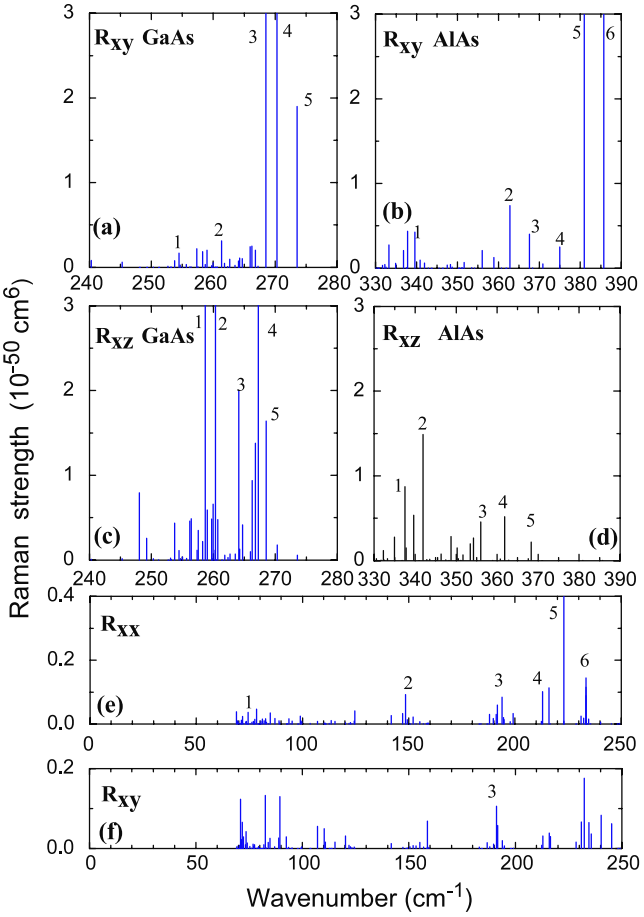

Figure 11. Calculated Raman mode strengths for 1×1 GaAs/AlAs(001) SL with cation intermixing (8 unit cells' approximation): (a) R_{xy} strengths for GaAs modes, (b) R_{xy} strengths for AlAs modes, (c) R_{xz} strengths for GaAs modes, (d) R_{xz} strengths for AlAs modes, (e) R_{xx} strengths, (f) R_{xy} strengths below 250 cm^{-1}.

(lower) frequencies due to the presence of lighter (heavier) Al (Ga) atoms in the same lattice plane. Furthermore, the fact that the frequencies of most of the optical modes are lying much closer each other with respect to the modes in the acoustic range renders the identification of their origin too risky and, for sure, more unambiguous. So, we will assign the frequencies of the optic modes only when necessary and only to the closest frequencies of the bulk modes, with any uncertainties involved with this procedure.

The calculated Raman spectrum for the longitudinal displacements of the vibrational modes is shown in figure 10(a). Due to the small degree of disorder, the spectrum in the acoustic range is very similar to the spectrum for the perfect 1×1 SL (figure 4, solid lines), although in the whole acoustic range, up to 200 cm^{-1}, there exists weak Raman activity. The peak b′, solid line, figure 10(a), originates mainly from the LA(X) longitudinal mode at 223 cm^{-1}, but with significant contributions from the modes at 213 and 216 cm^{-1} (labeled as 4, 5 and 6 in figure 11(e)). These modes originate from the LA(L) points. The weak activity at 200 cm^{-1} results from a group of mixed modes extending from 191 to 199.8 cm^{-1} (labeled as 3 in figures 11(e) and (f)) and originating from the (0.5, 0.5, 0.0) $(2\pi/a)$ point of the original Brillouin zone. The broad structure at 80 cm^{-1}, labeled as a, solid lines, figure 10(a), is formed from the contributions of: (a) six modes originating from the 0, 0, 0.5) $(2\pi/a)$ point, (b) four modes originating from the TA(L) point and (c) twelve modes originating from the (0.5, 0.5, 0.0) $(2\pi/a)$ point of the original BZ.

In the optical frequency range, the calculated spectrum (solid line in figure 10(a)) is much closer to the corresponding experimental spectrum, since also the low energy asymmetries of the stronger modes c and e (solid line in figure 10(a)) are now reproduced. Furthermore, peaks c and e appear now at 270.3 cm^{-1} and 385.8 cm^{-1} and are the strongest modes in the frequency ranges of GaAs and AlAs, respectively. Peak c, apart from the contributions of the two almost longitudinal strong modes at 270.3 and 273.5 cm^{-1} (labeled as 4 and 5 in figure 11(a)), contains contributions from a mixed mode at 268.5 cm^{-1} (labeled as 3 in figure 11(a)) as well as from the longitudinal component of the mixed modes with frequencies from 250 to 267.23 cm^{-1} (see figure 11(a)). We mention that these modes have frequencies close to the frequencies of the optical modes of the bulk GaAs at all the points that are folded to the center of the new BZ. Finally, some of these mixed modes with R_{xy} activity are mainly transverse modes but with a strength about two orders of magnitude weaker with respect to the strength of the 268.5 cm^{-1} (labeled as 5 in figure 11(c)). This is the case for the modes at 258.7, 260.3, 264 and 267.3 cm^{-1} (labeled as 1, 2, 3 and 4 in figure 11(c)).

The calculated peak e of LO(Γ) of AlAs at 385.8 cm^{-1} (solid line in figure 10(a)) also contains a contribution from the

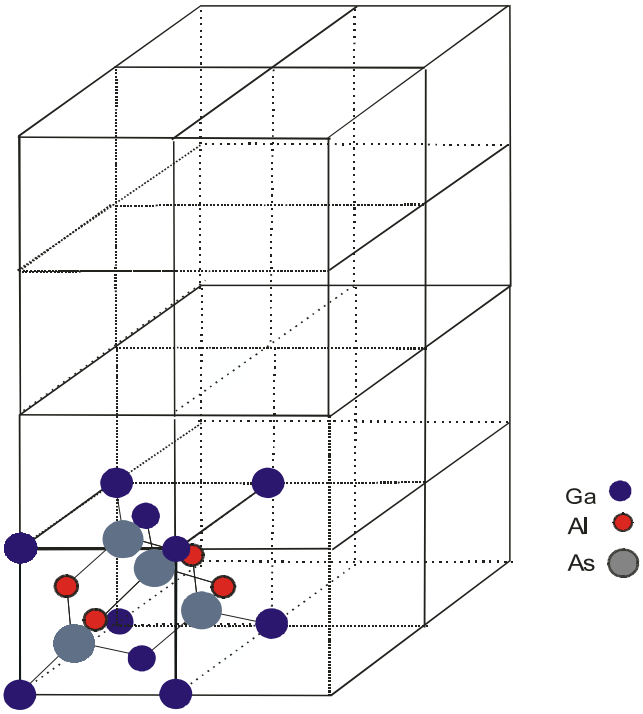

Figure 12. Supercell containing 16 zinc blende unit cells (2 along the x and y axes and 4 along the z axes). Translation of the tetragonal unit cell (lower left corner) in the space gives the structure of the perfect GaAs/AlAs(001) SL.

mode at 381.0 cm^{-1}. Both modes are longitudinal with small transverse displacements and are almost of the same strengths. Peak f at 338 cm^{-1} is due to a group of mixed modes labeled 1 in figures 11(b) and (d). The frequencies of these modes are close to the frequencies of the optical modes of the bulk AlAs at points (0.5, 0.5, 0.0) ($2\pi/a$) and (0.5, 0.0, 0.0) ($2\pi/a$). The asymmetric g peak, (solid line in figure 10(a)) originates mainly from the two mixed modes at 362.8 and 367.6 cm^{-1} (labeled as 2 and 3 in figure 11(b) or 4 and 5 in figure 11(d)). The frequencies of these modes are close to the frequencies of the optical modes of bulk AlAs at the points (0.0, 0.0, 0.0) ($2\pi/a$) (363.7 cm^{-1}), (1.0, 0.5, 0.0) ($2\pi/a$) (365.8 cm^{-1}) and (0.5, 0.5, 0.5) ($2\pi/a$) (366.8 cm^{-1}).

5.3.2. Supercell with 128 atoms. As a further step, we described the 1 × 1 SL with a new elementary cell defined by

$$\mathbf{a}_1 = 2a\mathbf{i} \qquad \mathbf{a}_2 = 2a\mathbf{j} \qquad \mathbf{a}_3 = 4a\mathbf{k}$$

where $a = 5.65$ A (figure 12). This new cell contains 16 zinc blende unit cells, two along the x, two along the y and four along the z axis. This cell contains 64 cations and 64 anions. Again, each horizontal cation (anion) lattice plane contains 8 cations (anions) with the following intermixing scheme of the cation lattice planes along the z axis: (in parentheses is quoted the height of the lattice plane). 6Ga–2Al (0), 5Al–3Ga ($a/2$), 6Ga–2Al (a), 6Al–2Ga ($3a/2$), 7Al–1Ga ($2a$), 6 Ga–2Al ($5a/2$), 6Al–2Ga ($3a$) and 5Ga–3Al ($7a/2$).

For this case, the symmetry space group is the C_1 space group of the triclinic system, while the points of the original Brillouin zone folded to the center of the new smaller Brillouin zone are: (a) the Γ point (0, 0, 0), (b) two (0, 0, 0.25) points, (c) six points equivalent to the point (0.5, 0, 0), (d) two points equivalent to the (0, 0, 0.75), (e) three points equivalent to the X point (1, 0, 0), (f) four points equivalent to the L point (0.5, 0.5, 0.5), (g) twelve points equivalent to the point (0.5, 0.5, 0) of the Σ direction, (h) six points of the Z direction equivalent to the W point (1, 0.5, 0), (i) four points equivalent to the (1, 0.25, 0) of the same direction, (j) eleven points (0.5, 0.25, 0.0), (k) six points (0.5, 0.75, 0.0) and (l) seven (0.5, 0.5, 0.25) points. The dynamical matrix for this case is a 384 × 384 matrix which is diagonalized to obtain the eigenvectors and eigenfrequencies of the disordered SL.

The calculated Raman spectrum for the modes with longitudinal displacements is shown in figure 10(b). The agreement between theory and experiment is very satisfactory. In the low frequency range there appears a broad structure from 70 to 100 cm^{-1}, peak a, of the solid line in figure 10(b). This structure is formed from about 100 weak modes in this frequency range. Peak b, close to 200 cm^{-1}, consists of about 28 modes with frequencies ranging from 180 to 220 cm^{-1}. Both peaks are formed by modes with weak R_{xx} activity, clearly dominating over the R_{xy} activity in this range, as can be deduced from figures 13(e) and (f).

Peak c appears now at 271.1 cm^{-1} (spike 2 in figure 13(a)). Even the strongest mode in this range has frequency 273.3 cm^{-1}, spike 3 in figure 13(a). In the formation of this peak the mode at 269.5 cm^{-1} (spike 1 in figure 13(a)), which is a mixed mode with significant R_{xy} and R_{xz} strengths (spike 1 in figure 13(c)),contributes up to 30%. Concerning its origination, most probably this mode originates mainly from the (1.0, 0.5, 0.0) or (0.5, 0.25, 0.0) point of the BZ. Further weak contributions to peak c are coming from the mixed modes at 269.2, 268.4 and 268.0 cm^{-1}, as well as from the modes at 256.2 and 256.4 cm^{-1} which are mainly transverse modes. Furthermore, as far as the origin of contributing modes is concerned, probably the former three modes originate from the highest frequency mode of the bulk GaAs (274.8 cm^{-1}) occurring at (0.50, 0.25, 0.00) of the original BZ, while the two latter modes are from the optical mode of the same binary either from the point (0.50, 0.50, 0.25) with frequency 260.3 cm^{-1} or from the point (0.50, 0.50, 0.00) with frequency 260.1 cm^{-1}.

Finally, peak e (solid lines, figure 10(b)) appears now at 381.9 cm^{-1}, with the strongest contributing mode at 386.1 cm^{-1}. The left asymmetry h is an outcome from two modes with frequencies at 375.4 and 375.9 cm^{-1}. All these four modes are almost purely longitudinal modes. Peaks f and g at 342.7 and 362 cm^{-1} originate from mixed, mainly transverse, modes. The frequencies nearby to 342 cm^{-1} are close to the optical frequency modes of bulk AlAs at the points (0.50, 0.50, 0.00) (335.9 cm^{-1}) and (0.50, 0.25, 0.00) (334.9 cm^{-1}). Similarly, the frequencies around 362 cm^{-1} are close to the optical frequency modes of bulk AlAs at the points (0.50, 0.50, 0.50) (366.8 cm^{-1}) and (0.50, 0.50, 0.25) (366.7 cm^{-1}) of the BZ, implying thus their nature and origination.

For the sake of completeness, we mention that former calculations, in order to describe the 1 × 1 SL, have used unit

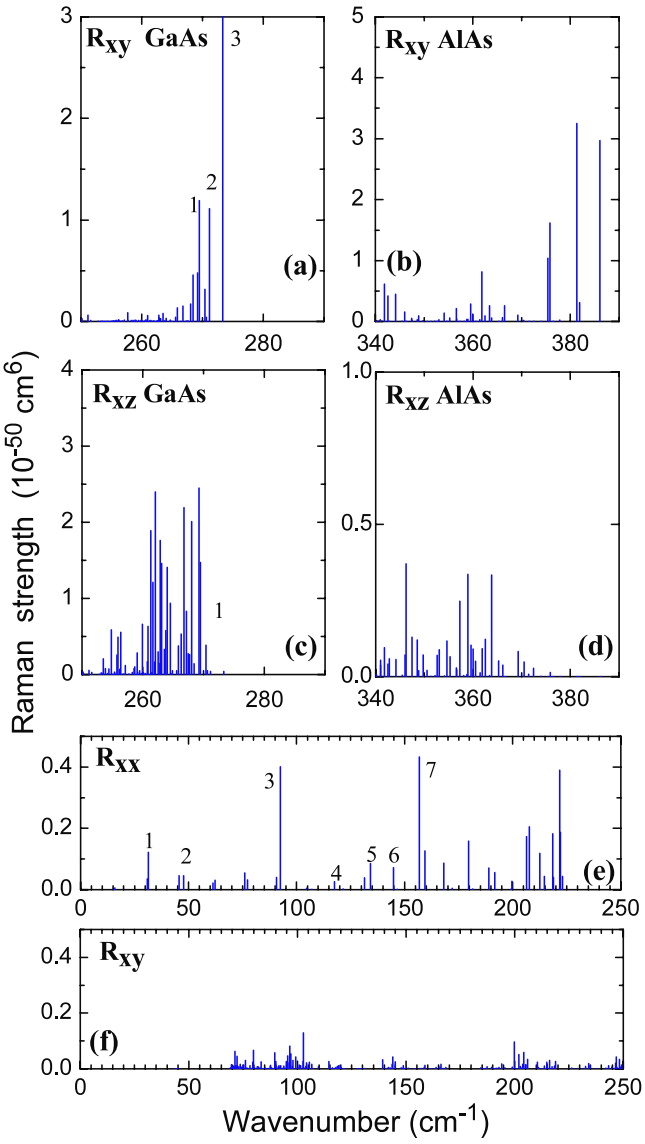

Figure 13. Calculated Raman mode strengths for the 1 × 1 GaAs/AlAs(001) SL with cation intermixing (16 unit cells approximation): (a) R_{xy} strengths for GaAs modes, (b) R_{xy} strengths for AlAs modes, (c) R_{xz} strengths for GaAs modes, (d) R_{xz} strengths for AlAs modes, (e) R_{xx} strengths, (f) R_{xy} strengths below 250 cm^{-1}.

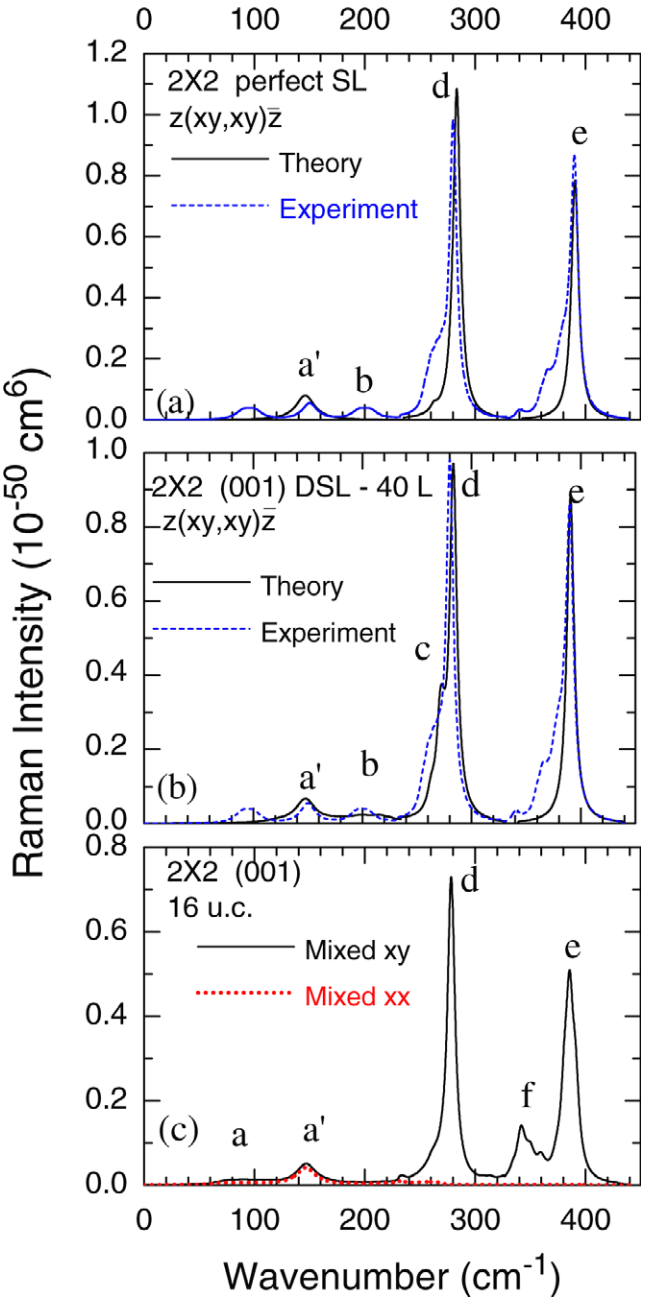

Figure 14. Calculated Raman spectra for GaAs/AlAs(001): (a) calculated for the perfect 2 × 2 SL, (b) calculated spectrum (solid lines) with 40 layers (disordered sequence) and the corresponding experimental spectrum in backscattering geometry. (c) Spectrum calculated with cation intermixing using an elementary supercell containing 16 zinc blende unit cells. Dotted lines in (a) are the corresponding experimental spectrum, while in (b) is the R_{xx} mode strengths.

cells containing only 16 atoms [25]. These calculations have found the frequency of the strongest LO mode of GaAs as 1 × 1 268 cm^{-1} and 400 cm^{-1} for the strongest LO mode of AlAs. Both values disagree with the experimental ones, especially that of the AlAs band.

6. $(GaAs)_2/(AlAs)_2$(001) perfect SL

Figure 14(a) (solid line) displays the calculated Raman spectrum for the 2 × 2 GaAs/AlAs(001) perfect superlattice with ideal interfaces. The calculation is carried out for zero wavevector along the superlattice axis only for the modes active in backscattering geometry $Z(X+Y, X+Y)\bar{Z}$, e.g. longitudinal modes with A_1 and B_2 symmetry. The two strong peaks d and e correspond to the B_2 LO(Γ) of GaAs at 283.3 cm^{-1} and B_2 LO(Γ) of AlAs at 390.4 cm^{-1}. The corresponding experimental peaks appear at 280 cm^{-1} and 389 cm^{-1} for GaAs and AlAs, respectively [9, 10]. The peak b′ present in the spectrum of the perfect 1 × 1 (001) SL (solid line in figure 4), and which corresponds to the longitudinal A_1 mode at 223 cm^{-1}, is absent in the 2 × 2 (001) SL, for the reason that it has now zero activity.

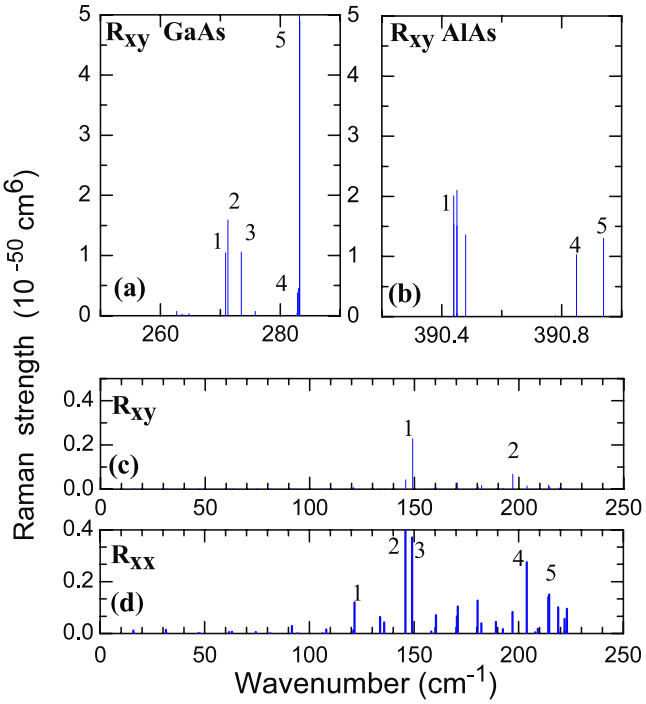

Figure 15. Calculated Raman mode strengths for 2 × 2 GaAs/AlAs(001) SL with disordered layer sequence (40 layers, 20 of GaAs and 20 of AlAs): (a) R_{xy} strengths for GaAs modes, (b) R_{xy} strengths for AlAs modes, (c) R_{xy} strengths and (d) R_{xx} strengths below 250 cm^{-1}.

6.1. $(GaAs)_2/(AlAs)_2(001)$ disordered layer superlattices (DLSLs)

In order to improve our description for the 2 × 2 GaAs/AlAs(001) SL Raman spectrum, we assume again a supercell, containing the following disordered layer sequence: GaAsAlAsAlAsGaAs/AlAsGaAsAlAsAlAs/GaAsGaAsAlAs AlAs/GaAsGaAsAlAsAlAs/GaAsGaAsAlAsGaAs/AlAsGaAs AlAsAlAs/GaAsGaAsAlAsAlAs/GaAsGaAsAlAsAlAs/GaAs GaAsAlAsAlAs/GaAsGaAsAlAsAlAs/.

The calculated spectrum for this SL for the Z(X + Y, X + Y)$\bar{Z}$ backscattering geometry is displayed in figure 14(b). Concerning the acoustic frequency range, the peak a′ appears at 148.4 cm^{-1} originating from the (0.50, 0.00, 0.00) point of the original BZ In this frequency range. In the experimental spectrum a weak activity is present close to 200 cm^{-1} (dotted line, figure 14(a)) which originates from the (0.75, 0.00, 0.00) point, while the LA(X) mode at 223 cm^{-1} does not form any peak. In the GaAs optical range, peak c appears at 271.3 cm^{-1} and peak d at 283.4 cm^{-1}, and in the AlAs optical range, peak e appears at 390.5 cm^{-1}. These frequencies are identical to the values found for the corresponding peaks in the case of the perfect 2 × 2 SL. Peak c is formed by the contributions of the modes labeled 1–3, figure 15(a), while peaks d and e are formed by the contributions of the modes labeled 4–5 for the GaAs layer, figure 15(a), and 1–5 for the AlAs layer, figure 15(b). In figures 15(c) and (d) are shown the strengths of the longitudinal modes below 250 cm^{-1} with R_{xy} and R_{xx} strengths, respectively.

6.2. $(GaAs)_2/(AlAs)_2(001)$ SLs with disordered lattice sites (cation intermixing)

As a final step, we described the 2 × 2 SL with a new elementary cell defined by

$$\mathbf{a}_1 = 2a\mathbf{i} \qquad \mathbf{a}_2 = 2a\mathbf{j} \qquad \mathbf{a}_3 = 4a\mathbf{k}$$

where $a = 5.65$ A. This new cell now contains 16 zinc blende unit cells, two along the x, two along the y and four along the z axis. This cell contains 64 cations and 64 anions. Again, each parallel to the interface cation (anion) lattice plane contains 8 cations (anions) and the intermixing scheme of the cation lattice planes along the z axis: (in parentheses is quoted the height of the lattice plane): 7Ga–1Al (0), 7Ga–1Al ($a/2$), 7AlA–1Ga (a), 7Al–1Ga ($3a/2$), 7Ga–1Al ($2a$), 7 Ga–1Al ($5a/2$), 6Al–2Ga ($3a$), 8Al–0 Ga ($7a/2$).

In figure 14(c) is displayed the calculated Raman spectrum for such an SL traced in the Z(X + Y, X + Y)$\bar{Z}$ backscattering geometry. The main finding in this description is the absence of the structure at 200 cm^{-1} and the weak Raman activity below and above that frequency. Also, the LA(X) mode at 223 cm^{-1} does not form any peak because, even active, its strength is very weak. In the acoustic frequency range, the peak a′ appears at 147.2 cm^{-1}, which originates from the (0.5, 0, 0,) point of the BZ. This broad structure of the peak a′ lying between 140 and 160 cm^{-1} is formed from contributions of the points (0.50, 0.25, 0.00), (eight modes), (0.50, 0, 0) (six modes) and (1.0, 0.50, 0) (six modes).

In the GaAs optical range, peak d appears at 278.3 cm^{-1}, spike 2 in figure 16(a), which is redshifted by 5 cm^{-1} compared to the corresponding d peak frequency for the 2 × 2 disordered SL (solid lines in figure 14(b)). To the formation of peak d contributes the longitudinal mode at 277.6 cm^{-1} (spike 1 in figure 16(a)), possibly originating from the (0, 0, 0.25) point of the original BZ. The left asymmetry of the GaAs peak d is formed by contributions of over 20 weak mixed modes ranging from 240 to 270 cm^{-1}.

In the AlAs optical range, peak e (solid line in figure 14(c)) appears at the frequency of the strong, mainly longitudinal, mode at 385.6 cm^{-1} (spike 6 in figure 16(b)) with contribution of the weaker, again mainly longitudinal, mode at 381.1 cm^{-1} (spike 5 in figure 16(b)). The frequency of peak e is also redshifted by 4.9 cm^{-1} compared to the frequency of peak e (solid lines, figure 14(c)) for the 2 × 2 disordered Sl. Peak f, at the low energy of peak e, appears at 341.7 cm^{-1} and is comprised by contributions of modes with frequencies ranging from 340 to 350 cm^{-1} and possibly originating from the points (0.50, 0.25, 0.00) and (0.50, 0.50, 0.00) (marked as 1 and 2 in figure 16(b)).

In [25] has also been considered the 2 × 2 SL using unit cells with a very limited number of atoms. As for the case of the 1 × 1 SL, their theoretical results differ from the experimental, giving for the strongest LO mode of GaAs the value of 290 cm^{-1}, very close to that of the bulk crystal.

7. Conclusion

We have calculated in various degrees of disorder the vibrational modes and the Raman spectra of GaAs/AlAs(001)

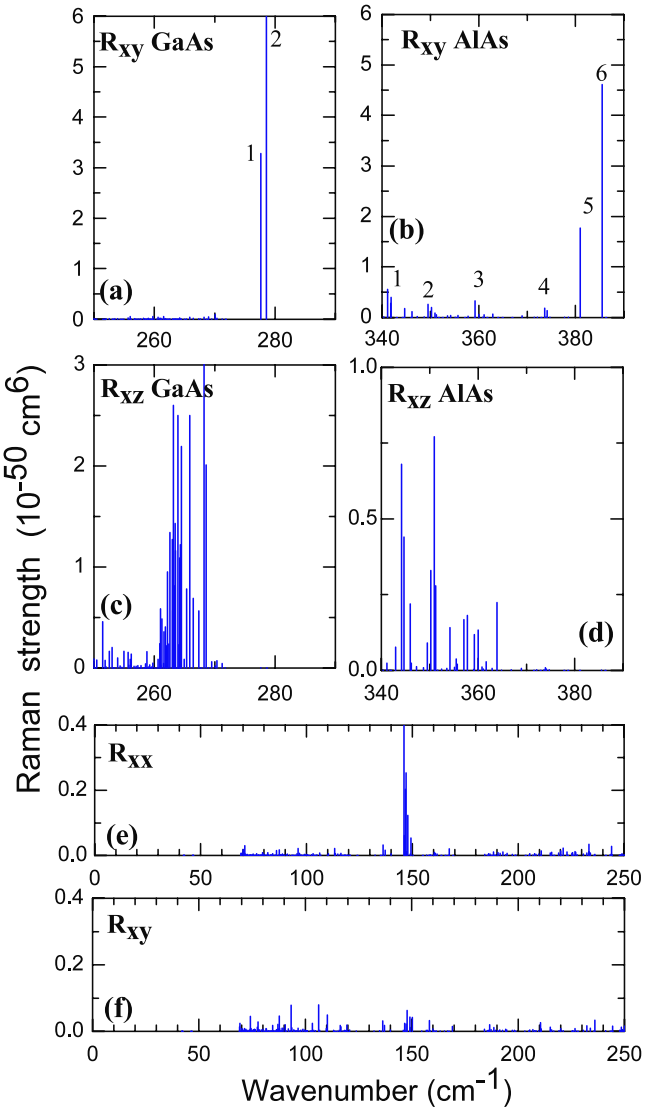

Figure 16. Calculated Raman mode strengths for 2 × 2 GaAs/AlAs(001) SL with cation intermixing (16 unit cells' approximation): (a) R_{xy} strengths for GaAs modes, (b) R_{xy} strengths for AlAs modes, (c) R_{xz} strengths for GaAs modes, (d) R_{xz} strengths for AlAs modes, (e) R_{xx} strengths, (f) R_{xy} strengths below 250 cm^{-1}.

SLs, starting from perfect SLs. Disorder degree has been simulated by approximating the SLs with large primitive cells. In the case of randomly intermixed cations, these large cells do not contain any symmetry elements and therefore all the vibrational modes are mixed modes and all of them, potentially, Raman-active.

Our results clearly show that the asymmetric profiles of the experimentally observed Raman lines in the optical frequency are due to active modes not only from the Δ direction, but from all the points of the Brillouin zone. An unambiguous assignment of the origin of these modes is a very risky and doubtful procedure, because of the very close lying mode frequencies as well as of their strong and different degrees of influence due to the cation intermixing. The high number of contributing modes in each Raman peak makes almost impossible their experimental resolution in the optical branch. On the other hand, in the acoustic frequency range the identification of their origin can be almost safely guessed.

Furthermore, we have shown that in some cases the frequency of the strongest Raman peak does not correspond to the mode with the highest frequency and largest Raman activity, but to a mode some times weaker and with frequency very close to that of the very strong one. This is the outcome of the superposition of the intensities of the neighboring modes. In addition, we have shown that the peak close to 200 cm^{-1}, known as the DALA mode, is not a disorder-activated LA(X) mode, but is formed by the contribution of modes originating from several points of several directions of the BZ, such as Δ, Σ, Z and Λ. Therefore, the LA(X) mode with frequency at 223.0 cm^{-1} is not always activated by disorder.

Acknowledgments

One of us (DB) would like to thank Professor Roger Fletcher, Dundee University, Scotland, for sending us an efficient function minimization code based on the Marquardt method [41].

References

[1] Jusserand B and Cardona M 1989 *Light Scattering in Solids V* (*Topics in Applied Physics*) vol 66, ed M Cardona and G Guntherondt (Berlin: Springer)
[2] Volodin V, Efremov M, Sachkov V and Preobrazhenski V 2001 *Nanotechnology* **12** 508
[3] Halsall M and Dawson P 1996 *J. Appl. Phys.* **81** 224
[4] Wang Z P, Han H X, Li G H, Jiang D S and Ploog K 1991 *Phys. Rev.* B **43** 12650
[5] Wang Z P, Jiang D S and Ploog K 1988 *Solid State Commun.* **65** 661
[6] Jusserand B, Paquet D and Mollot F 1989 *Phys. Rev. Lett.* **63** 2397
[7] Ishibashi A 1989 *NATO Advanced Research Workshop on Spectroscopy of Semiconductor Microstructures (Venice, May)*
[8] Ishibashi A, Itabashi M, Mori Y, Kaneko K, Kawado S and Watanabe N 1986 *Phys. Rev.* B **33** 2887
[9] Toriyama T, Kobayashi N and Horikoshi Y 1986 *Japan. J. Appl. Phys.* **25** 1895
[10] Nakayama M, Kubota K, Kato H, Chika S and Shano N 1985 *Solid State Commun.* **53** 493
[11] Jusserand B and Sapriel J 1981 *Phys. Rev.* B **24** 7194
[12] Barker A S, Merz J L Jr and Gossard A C 1978 *Phys. Rev.* B **17** 3181
[13] Popovic Z V, Cardona M, Richter E, Strauch D, Tapfer L and Ploog K 1989 *Phys. Rev.* B **40** 3040
[14] Popovic Z V, Cardona M, Richter E, Strauch D, Tapfer L and Ploog K 1989 *Phys. Rev.* B **40** 1207
[15] Popovic Z V, Cardona M, Richter E, Strauch D, Tapfer L and Ploog K 1990 *Phys. Rev.* B **41** 5904
[16] Colvard C, Gant T A, Klein M V, Merlin R, Fischer R, Morkoc H and Gossard A C 1985 *Phys. Rev.* B **31** 2080
[17] Colvard C, Merlin R, Klein M V and Gossard A C 1980 *Phys. Rev. Lett.* **45** 298
[18] Kanellis G 1987 *Phys. Rev.* B **35** 746
[19] Kechrakos D, Briddon P R and Inkson J C 1991 *Phys. Rev.* B **44** 9114
[20] Richter E and Strauch D 1987 *Solid State Commun.* **64** 867
[21] Jusserand B 1990 *Phys. Rev.* B **42** 7256

[22] Berdekas D 1991 Study of lattice dynamics of mixed crystals *PhD Thesis* Department of Physics, University of Thessaloniki, Thessaloniki, unpublished
[23] Yip S K and Chang Y C 1984 *Phys. Rev.* B **30** 7037
[24] Lambert K and Srivastava G P 1997 *Phys. Rev.* B **56** 13387
[25] Baroni St, Giannozzi P and Molinari E 1990 *Phys. Rev.* B **41** 3870
[26] Molinari E, Baroni St, Giannozzi P and Gironcoli St 1992 *Phys. Rev.* B **45** 4280
[27] Pandey R N, Sharma T P and Dayal B 1976 *J. Phys. Chem. Solids* **18** 329
[28] Kunc K and Bilz H 1976 *Solid State Commun.* **19** 1027
[29] Bilz H, Strauch D and Wehner R K 1984 *Light and Matter* (*Handbuch der Physik* vol XXV/2D) ed L Genzel (Berlin: Springer)
[30] Kanellis G, Kress W and Bilz H 1986 *Phys. Rev.* B **33** 8724
[31] Tubino R and Piseri L 1975 *Phys. Rev.* B **11** 5145
[32] Nakashima S, Katahama H, Nakakura Y and Mitsuishi A 1986 *Phys. Rev.* B **33** 5721
[33] Strauch D and Dorner B 1990 *J. Phys.: Condens. Matter* **2** 1457
[34] Dolling G and Waugh J L T 1965 *Lattice Dynamics* ed R F Wallis (Oxford: Pergamon)
[35] Monemar B 1973 *Phys. Rev.* B **8** 5711
Klein P B, Son J-J, Chang R K and Callender R H 1975 *Proc. 3th Int. Conf. on Light Scattering in Solids* ed M Balkanski, R C C Leite and S P S Porto, p 93
[36] Cowley R A 1971 *The Raman Effect* ed A Anderson (New York: Dekker) p 95
[37] Flytzanis C and Ducuing J 1969 *Phys. Rev.* **178** 1218
[38] Cardona M 1982 *Light Scattering in Solids II* ed M Cardona and G Guntherondt (Berlin: Springer)
[39] Flytzanis C 1972 *Phys. Rev.* B **6** 1264
[40] Castrillo P, Armelles G, Gonzalez L, Dominguez P S and Colombo L 1995 *Phys. Rev.* B **51** 1647
[41] Fletcher R 1971 A modified Marquardt subroutine for non linear least squares *AERE Harwell, R6799*